 CMES, vol.34, no.3, pp.273-300, 2008

Modeling of Intelligent Material Systems by the MLPG

J. Sladek[1], V. Sladek[2], P. Solek[1] and S.N. Atluri[3]

Abstract: A meshless method based on the local Petrov-Galerkin approach is proposed, to solve boundary and initial value problems of piezoelectric and magneto-electric-elastic solids with continuously varying material properties. Stationary and transient dynamic 2-D problems are considered in this paper. The mechanical fields are described by the equations of motion with an inertial term. To eliminate the time-dependence in the governing partial differential equations the Laplace-transform technique is applied to the governing equations, which are satisfied in the Laplace-transformed domain in a weak-form on small subdomains. Nodal points are spread on the analyzed domain, and each node is surrounded by a small circle for simplicity. The spatial variation of the displacements and the electric potential are approximated by the Moving Least-Squares (MLS) scheme. After performing the spatial integrations, one obtains a system of linear algebraic equations for unknown nodal values. The boundary conditions on the global boundary are satisfied by the collocation of the MLS-approximation expressions for the displacements and the electric potential at the boundary nodal points. The Stehfest's inversion method is applied to obtain the final time-dependent solutions.

Keyword: Meshless local Petrov-Galerkin method (MLPG), Moving least-squares interpolation, piezoelectric and piezomagnetic solids, Laplace-transform, Stehfest's inversion

1 Indroduction

Modern smart structures, made of piezoelectric and piezomagnetic materials, offer certain potential performance advantages over conventional ones, due to their capability of converting the energy from one type to other (among magnetic, electric, and mechanical) [Avellaneda and G. Harshe (1994); Berlingcourt et al. (1964);

[1] Institution of Construction and Architecture, Slovak Academy of Sciences, 84503 Bratislava, Slovakia, sladek@savba.sk
[2] Department of Mechanics, Slovak Technical University, Bratislava, Slovakia
[3] Department of Mechanical and Aerospace Engineering, University of California, Irvine, USA

Landau et al. (1984); Nan (1994)]. Earlier activities were focused on modeling piezoelectric problems [Tiersten (1969); Ha et al. (1992); Gaudenzi and Bathe (1995); Lee (1995); Chen and Lin (1995); Batra and Liang (1997); Ding and Liang (1999); Liew et al. (2002]. Later, there were also some efforts to model magneto-electric-elastic fields [Alshits et al. (1992); Chung and Ting (1995); Pan (2001); Liu et al. (2001); Wang and Shen (2002)]. Recently, increasing interest is devoted to fracture mechanics of piezoelectric [Beom and Atluri (1996, 2002), Gruebner et al. (2003); Govorukha and Kamlah (2004); Enderlein et al. (2005), Kuna (2006); Pan (1999); Gross et al. (2005); Garcia-Sanchez et al. (2005, 2007a); Saez et al. (2006); Sheng and Sze (2006)] and magneto-electric-elastic materials [Beom and Atluri (2003), Gao et al. (2003); Song and Sih (2003); Zhou et al. (2004); Hu et al. (2006); Wang et al. (2006); Tian and Gabbert (2005); Tian and Rajapakse, (2005); Garcia-Sanchez et al. (2007b); Wang and Mai (2007)]. Applications are mostly made under a static deformation assumption. Dynamic fracture analyses are being considered very seldom in literature.

While the piezoelectric and piezomagnetic effects are due to electro-elastic and magneto-elastic interaction, respectively, the magnetoelectric effect is the induction of the electrical polarization by magnetic field and the induction of magnetization by electric field via electro-magneto-elastic interactions. Magnetoelectric coupling plays an important role in the dynamic behaviour of certain materials, especially compounds which possess simultaneously ferroelectric and ferromagnetic phases [Eringen and Maugin, (1990)]. The electric and magnetic symmetry groups for certain crystals permit the piezoelectric and piezomagnetic as well as magnetoelectric effects. In centrosymmetric crystals neither of these effects exists. However, remarkably large magnetoelectric effects are observed for composites than for either composite constituent [Nan, (1994); Feng and Su, (2006)]. If the volume fraction of constituents is varying in a predominant direction we are talking about functionally graded materials (FGMs). Originally these materials have been introduced to benefit from the ideal performance of its constituents, e.g. high heat and corrosion resistance of ceramics on one side, and large mechanical strength and toughness of metals on the other side. A review on various aspects of FGMs can be found in the monograph of Suresh and Mortensen (1998). Later, the demand for piezoelectric materials with high strength, high toughness, low thermal expansion coefficient and low dielectric constant encourages the study of functionally graded piezoelectric materials [Zhu et al. (1995); Han et al. (2006)]. According the best of authors' knowledge there is available only one paper [Feng and Su, (2006)] with applications to continuously nonhomogeneous magneto-electric materials.

The solution of general boundary value problems for continuously nonhomogeneous magneto-electric-elastic solids requires advanced numerical methods due to

the high mathematical complexity. Besides this complication, the magnetic, electric and mechanical fields are coupled with each other in the constitutive equations. In spite of the great success of the finite element method (FEM) and boundary element method (BEM) as effective numerical tools for the solution of boundary value problems in mainly elastic solids, there is still a growing interest in the development of new advanced numerical methods. In recent years, meshless formulations are becoming popular due to their high adaptability and low costs to prepare input and output data in numerical analysis. The moving least squares (MLS) approximation is generally considered as one of many schemes to interpolate discrete data with a reasonable accuracy. The order of continuity of the MLS approximation is given by the minimum between the orders of continuity of the basis functions and that of the weight function. So continuity can be tuned to a desired value. In conventional discretization methods, the interpolation functions usually result in a discontinuity of secondary fields (gradients of primary fields) on the interfaces of elements. For modeling of continuously nonhomogeneous solids the approach based on piecewise continuous elements can bring some inaccuracies. Therefore, modeling based on C^1 continuity, such as in meshless methods, is expected to be more accurate than conventional discretization techniques. The meshless or generalized FEM methods are also very convenient for modeling of cracks. One can embed particular enrichment functions at the crack tip so the stress intensity factor can be predicted accurately [Fleming et al, (1997)].

A variety of meshless methods has been proposed so far, with some of them being applied only to piezoelectric problems [Ohs and Aluru, (2001); Liu et al., (2002)]. They can be derived from a weak-form formulation either on the global domain or on a set of local subdomains. In the global formulation, background cells are required for the integration of the weak-form. In methods based on local weak-form formulation, no background cells are required and therefore they are often referred to as truly meshless methods. The meshless local Petrov-Galerkin (MLPG) method is a fundamental base for the derivation of many meshless formulations, since trial and test functions can be chosen from different functional spaces [Zhu et al. (1998); Atluri et al. (2000); Atluri (2004); Sladek et al., (2000, 2001, 2003a,b); Sellountos and Polyzos (2003); Sellountos et al., (2005)]. Recently, the MLPG method with a Heaviside step function as the test functions [Atluri et al. (2003); Sladek et al., (2004, 2006a)] has been applied to solve two-dimensional (2-D) homogeneous and continuously nonhomogeneous piezoelectric solids [Sladek et al., (2006b, 2007a,b)].

In the present paper, the MLPG method is applied to 2-D continuously nonhomogeneous piezoelectric and magneto-electric-elastic solids. The coupled governing partial differential equations are satisfied in a weak form on small fictitious subdo-

mains. Nodal points are introduced and spread on the analyzed domain and each node is surrounded by a small circle for simplicity, but without loss of shape generality. For a simple shape of subdomains, such as a circle used in this paper, numerical integrations over them can be easily carried out. The integral equations have a very simple nonsingular form. The spatial variations of the displacements and the electric potential are approximated by the moving least-squares scheme [Belytschko et al., (1996); Atluri, (2004)]. After performing the spatial integrations, a system of linear algebraic equations for the unknown nodal values is obtained.

2 Local boundary integral equations

Basic equations of phenomenological theory of nonconducting elastic materials consist of the governing equations (Maxwell's equations, the balance of momentum) and the constitutive relationships. An electro-elastic problem can be considered as a special case of a general magneto-electric-elastic problem. Therefore, a formulation is given here for a general magneto-electric-elastic problem. The governing equations, which are complemented by the boundary and initial conditions, should be solved for the unknown primary field variables such as the elastic displacement vector field $u_i(\mathbf{x},\tau)$, the electric potential $\psi(\mathbf{x},\tau)$ (or its gradient, called the electric vector field $E_i(\mathbf{x},\tau)$), and the magnetic potential $\mu(\mathbf{x},\tau)$ (or its gradient, called the magnetic intensity field $H_i(\mathbf{x},\tau)$). The constitutive equations correlate the primary fields $\{u_i,E_i,H_i\}$ with the secondary fields $\{\sigma_{ij},D_i,B_i\}$which are the stress tensor field, the electric displacement vector field, and the magnetic induction vector field, respectively. The governing equations give not only the relationships between conjugated fields in each of the pairs$(\sigma_{ij},\varepsilon_{ij})$, (D_i,E_i), (B_i,H_i), but describe also the electro-magneto-elastic interactions in the phenomenological theory of continuous solids.

Taking into account the typical material coefficients, it can be found that characteristic frequencies for elastic and electromagnetic processes are $f_{el}=10^4$Hz and $f_{elm}=10^7$Hz, respectively. Thus, if we consider such bodies under transient loadings, with temporal changes corresponding to f_{el}, the changes of the electromagnetic fields can be assumed to be immediate, or in other words the electromagnetic fields can be considered like quasi-static [Parton and Kudryavtsev, (1988)]. Then, the Maxwell equations are reduced to two scalar equations

$$D_{j,j}(\mathbf{x},\tau)=0, \tag{1}$$

$$B_{j,j}(\mathbf{x},\tau)=0, \tag{2}$$

The rest of the vector Maxwell's equations in quasi-static approximation, $\nabla\times\mathbf{E}=0$ and $\nabla\times\mathbf{H}=0$, are satisfied identically by an appropriate representation of the fields

$\mathbf{E}(\mathbf{x},\tau)$ and $\mathbf{H}(\mathbf{x},\tau)$ as gradients of scalar electric and magnetic potentials $\psi(\mathbf{x},\tau)$ and $\mu(\mathbf{x},\tau)$, respectively,

$$E_j(\mathbf{x},\tau) = -\psi_{,j}(\mathbf{x},\tau), \tag{3}$$

$$H_j(\mathbf{x},\tau) = -\mu_{,j}(\mathbf{x},\tau). \tag{4}$$

To complete the set of governing equations, eqs. (1) and (2), one needs to use the equation of motion in an elastic continuum:

$$\sigma_{ij,j}(\mathbf{x},\tau) + X_i(\mathbf{x},\tau) = \rho\ddot{u}_i(\mathbf{x},\tau), \tag{5}$$

where $\ddot{u}_i$, ρ and X_i denote the acceleration of displacements, the mass density, and the body force vector, respectively. A comma after a quantity represents the partial derivatives of the quantity and a dot is used for the time derivative.

Finally, we extend the constitutive equations involving the general electro-magneto-elastic interaction [Nan, (1994)] to media with spatially dependent material coefficients for continuously non-homogeneous media

$$\sigma_{ij}(\mathbf{x},\tau) = c_{ijkl}(\mathbf{x})\varepsilon_{kl}(\mathbf{x},\tau) - e_{kij}(\mathbf{x})E_k(\mathbf{x},\tau) - d_{kij}(\mathbf{x})H_k(\mathbf{x},\tau), \tag{6}$$

$$D_j(\mathbf{x},\tau) = e_{jkl}(\mathbf{x})\varepsilon_{kl}(\mathbf{x},\tau) + h_{jk}(\mathbf{x})E_k(\mathbf{x},\tau) + \alpha_{jk}(\mathbf{x})H_k(\mathbf{x},\tau), \tag{7}$$

$$B_j(\mathbf{x},\tau) = d_{jkl}(\mathbf{x})\varepsilon_{kl}(\mathbf{x},\tau) + \alpha_{kj}(\mathbf{x})E_k(\mathbf{x},\tau) + \gamma_{jk}(\mathbf{x})H_k(\mathbf{x},\tau), \tag{8}$$

with the strain tensor ε_{ij} being related to the displacements u_i by

$$\varepsilon_{ij} = \frac{1}{2}\left(u_{i,j} + u_{j,i}\right). \tag{9}$$

The functional coefficients $c_{ijkl}(\mathbf{x})$, $h_{jk}(\mathbf{x})$, and $\gamma_{jk}(\mathbf{x})$ are the elastic coefficients, dielectric permittivities, and magnetic permeabilities, respectively; $e_{kij}(\mathbf{x})$, $d_{kij}(\mathbf{x})$, and $\alpha_{jk}(\mathbf{x})$ are the piezoelectric, piezomagnetic, and magnetoelectric coefficients, respectively. Owing to transient loadings, inertial effects and the coupling of fields, the elastic fields as well as electromagnetic fields are time dependent, even though the fields E_i and H_i are treated through a quasi-static approximation.

In the case of certain crystal symmetries, one can formulate also the plane-deformation problems [Parton and Kudryavtsev, (1988)]. For instance, in the crystals of hexagonal symmetry with x_3 being the 6-order symmetry axis and assuming $u_2 = 0$ as well as the independence on x_2, i.e. $(\cdot)_{,2} = 0$, we have $\varepsilon_{22} = \varepsilon_{23} = \varepsilon_{12} = E_2 =$

$H_2 = 0$. Then, the constitutive equations (6) - (8) are reduced to the following form

$$\begin{bmatrix}\sigma_{11}\\ \sigma_{33}\\ \sigma_{13}\end{bmatrix} = \begin{bmatrix}c_{11} & c_{13} & 0\\ c_{13} & c_{33} & 0\\ 0 & 0 & c_{44}\end{bmatrix}\begin{bmatrix}\varepsilon_{11}\\ \varepsilon_{33}\\ 2\varepsilon_{13}\end{bmatrix} - \begin{bmatrix}0 & e_{31}\\ 0 & e_{33}\\ e_{15} & 0\end{bmatrix}\begin{bmatrix}E_1\\ E_3\end{bmatrix} - \begin{bmatrix}0 & d_{31}\\ 0 & d_{33}\\ d_{15} & 0\end{bmatrix}\begin{bmatrix}H_1\\ H_3\end{bmatrix}$$
$$= \mathbf{C}(\mathbf{x})\begin{bmatrix}\varepsilon_{11}\\ \varepsilon_{33}\\ 2\varepsilon_{13}\end{bmatrix} - \mathbf{L}(\mathbf{x})\begin{bmatrix}E_1\\ E_3\end{bmatrix} - \mathbf{K}(\mathbf{x})\begin{bmatrix}H_1\\ H_3\end{bmatrix}, \quad (10)$$

$$\begin{bmatrix}D_1\\ D_3\end{bmatrix} = \begin{bmatrix}0 & 0 & e_{15}\\ e_{31} & e_{33} & 0\end{bmatrix}\begin{bmatrix}\varepsilon_{11}\\ \varepsilon_{33}\\ 2\varepsilon_{13}\end{bmatrix} + \begin{bmatrix}h_{11} & 0\\ 0 & h_{33}\end{bmatrix}\begin{bmatrix}E_1\\ E_3\end{bmatrix} + \begin{bmatrix}\alpha_{11} & 0\\ 0 & \alpha_{33}\end{bmatrix}\begin{bmatrix}H_1\\ H_3\end{bmatrix}$$
$$= \mathbf{G}(\mathbf{x})\begin{bmatrix}\varepsilon_{11}\\ \varepsilon_{33}\\ 2\varepsilon_{13}\end{bmatrix} + \mathbf{H}(\mathbf{x})\begin{bmatrix}E_1\\ E_3\end{bmatrix} + \mathrm{A}(\mathbf{x})\begin{bmatrix}H_1\\ H_3\end{bmatrix}, \quad (11)$$

$$\begin{bmatrix}B_1\\ B_3\end{bmatrix} = \begin{bmatrix}0 & 0 & d_{15}\\ d_{31} & d_{33} & 0\end{bmatrix}\begin{bmatrix}\varepsilon_{11}\\ \varepsilon_{33}\\ 2\varepsilon_{13}\end{bmatrix} + \begin{bmatrix}\alpha_{11} & 0\\ 0 & \alpha_{33}\end{bmatrix}\begin{bmatrix}E_1\\ E_3\end{bmatrix} + \begin{bmatrix}\gamma_{11} & 0\\ 0 & \gamma_{33}\end{bmatrix}\begin{bmatrix}H_1\\ H_3\end{bmatrix}$$
$$= \mathbf{R}(\mathbf{x})\begin{bmatrix}\varepsilon_{11}\\ \varepsilon_{33}\\ 2\varepsilon_{13}\end{bmatrix} + \mathbf{A}(\mathbf{x})\begin{bmatrix}E_1\\ E_3\end{bmatrix} + \mathbf{M}(\mathbf{x})\begin{bmatrix}H_1\\ H_3\end{bmatrix}, \quad (12)$$

Recall that σ_{22} does not influence the governing equations, although it is not vanishing in general, since$\sigma_{22} = c_{12}\varepsilon_{12} + c_{13}\varepsilon_{33} - e_{13}E_3$.

The following essential and natural boundary conditions are assumed for the mechanical field

$$u_i(\mathbf{x},\tau) = \tilde{u}_i(\mathbf{x},\tau), \quad \text{on } \Gamma_u,$$
$$t_i(\mathbf{x},\tau) = \sigma_{ij}n_j = \tilde{t}_i(\mathbf{x},\tau), \quad \text{on } \Gamma_t, \quad \Gamma = \Gamma_u \cup \Gamma_t.$$

For the electrical field, we assume

$$\psi(\mathbf{x},\tau) = \tilde{\psi}(\mathbf{x},\tau), \quad \text{on } \Gamma_p,$$
$$n_i(\mathbf{x})D_i(\mathbf{x},\tau) \equiv Q(\mathbf{x},\tau) = \tilde{Q}(\mathbf{x},\tau), \quad \text{on } \Gamma_q, \quad \Gamma = \Gamma_p \cup \Gamma_q$$

and for the magnetic field

$$\mu(\mathbf{x},\tau) = \tilde{\mu}(\mathbf{x},\tau), \quad \text{on } \Gamma_a,$$
$$n_i(\mathbf{x})B_i(\mathbf{x},\tau) \equiv S(\mathbf{x},\tau) = \tilde{S}(\mathbf{x},\tau), \quad \text{on } \Gamma_b, \quad \Gamma = \Gamma_a \cup \Gamma_b$$

where Γ_u is the part of the global boundary Γ with prescribed displacements, while on Γ_t, Γ_p, Γ_q, Γ_a and Γ_b the traction vector, the electric potential, the normal component of the electric displacement vector, the magnetic potential and the magnetic flux are prescribed, respectively. Recall that $\tilde{Q}(\mathbf{x},\tau)$ can be considered approximately as the surface density of free charge, provided that the permittivity of the solid is much greater than that of the surrounding medium (vacuum).

The initial conditions for the mechanical displacements are assumed as

$$u_i(\mathbf{x},\tau)|_{\tau=0} = u_i(x,0) \text{ and } \dot{u}_i(\mathbf{x},\tau)|_{\tau=0} = \dot{u}_i(x,0) \text{ in } \Omega.$$

The Laplace transform technique is applied to eliminate the time variable in the differential equation. Applying to the governing equations (5) one obtains

$$\bar{\sigma}_{ij,j}(\mathbf{x},p) - \rho(\mathbf{x})p^2\bar{u}_i(\mathbf{x},p) = -\bar{F}_i(\mathbf{x},p), \tag{13}$$

where p is the Laplace-transform parameter and

$$\bar{F}_i(\mathbf{x},p) = \bar{X}_i(\mathbf{x},p) + pu_i(\mathbf{x},0) + \dot{u}_i(\mathbf{x},0),$$

is the re-defined body force in the Laplace-transformed domain with the initial boundary conditions for the displacements $u_i(\mathbf{x},0)$ and velocities $\dot{u}_i(\mathbf{x},0)$. Recall that the subscripts take now values $i \in \{1,3\}$.

Instead of writing the global weak-form for the above governing equations, the MLPG method constructs a weak-form over the local fictitious subdomains such as Ω_s, which is a small region constructed for each node inside the global domain [Atluri, (2004)]. The local subdomains overlap each other, and cover the whole global domain Ω. The local subdomains could be of any geometrical shape and size. In the present paper, the local subdomains are taken to be of a circular shape for simplicity. The local weak-form of the governing equation (13) can be written as

$$\int_{\Omega_s} \left[\bar{\sigma}_{ij,j}(\mathbf{x},p) - \rho(\mathbf{x})p^2\bar{u}_i(\mathbf{x},p) + \bar{F}_i(\mathbf{x},p)\right] u^*_{ik}(\mathbf{x})d\Omega = 0, \tag{14}$$

where $u^*_{ik}(\mathbf{x})$ is a test function.

Applying the Gauss divergence theorem to eq. (14) one obtains

$$\int_{\partial\Omega_s} \bar{\sigma}_{ij}(\mathbf{x},p)n_j(\mathbf{x})u^*_{ik}(\mathbf{x})d\Gamma - \int_{\Omega_s} \bar{\sigma}_{ij}(\mathbf{x},p)u^*_{ik,j}(\mathbf{x})d\Omega + \int_{\Omega_s} \left[\bar{F}_i(\mathbf{x},p) - \rho(\mathbf{x})p^2\bar{u}_i(\mathbf{x},p)\right] u^*_{ik}(\mathbf{x})d\Omega = 0, \tag{15}$$

where $\partial\Omega_s$ is the boundary of the local subdomain which consists of three parts $\partial\Omega_s = L_s \cup \Gamma_{st} \cup \Gamma_{su}$ [Atluri, (2004)]. Here, L_s is the local boundary that is totally inside the global domain, Γ_{st} is the part of the local boundary which coincides with the global traction boundary, i.e., $\Gamma_{st} = \partial\Omega_s \cap \Gamma_t$, and similarly Γ_{su} is the part of the local boundary that coincides with the global displacement boundary, i.e., $\Gamma_{su} = \partial\Omega_s \cap \Gamma_u$.

By choosing a Heaviside step function as the test function $u^*_{ik}(\mathbf{x})$ in each subdomain as

$$u^*_{ik}(\mathbf{x}) = \begin{cases} \delta_{ik} & \text{at } \mathbf{x} \in \Omega_s \\ 0 & \text{at } \mathbf{x} \notin \Omega_s \end{cases},$$

the local weak-form (15) is converted into the following local boundary-domain integral equations

$$\int_{L_s+\Gamma_{su}} \bar{t}_i(\mathbf{x},p)d\Gamma - \int_{\Omega_s} \rho(\mathbf{x})p^2\bar{u}_i(\mathbf{x},p)d\Omega = -\int_{\Gamma_{st}} \bar{\bar{t}}_i(\mathbf{x},p)d\Gamma - \int_{\Omega_s} \bar{F}_i(\mathbf{x},p)d\Omega. \tag{16}$$

Equation (16) is recognized as the overall force equilibrium conditions on the subdomain Ω_s. Note that the local integral equation (16) is valid for both the homogeneous and nonhomogeneous solids. Nonhomogeneous material properties are included in eq. (16) through the elastic, piezoelectric and piezomagnetic coefficients in the traction components.

Similarly, the local weak-form of the governing equation (2) can be written as

$$\int_{\Omega_s} \bar{D}_{j,j}(\mathbf{x},p)v^*(\mathbf{x})d\Omega = 0, \tag{17}$$

where $v^*(\mathbf{x})$ is a test function.

Applying the Gauss divergence theorem to the local weak-form (17) and choosing the Heaviside step function as the test function $v^*(\mathbf{x})$ one can obtain

$$\int_{L_s+\Gamma_{sp}} \bar{Q}(\mathbf{x},p)d\Gamma = -\int_{\Gamma_{sq}} \bar{\bar{Q}}(\mathbf{x},p)d\Gamma, \tag{18}$$

where

$$\bar{Q}(\mathbf{x},p) = \bar{D}_j(\mathbf{x},p)n_j(\mathbf{x}) = \left[e_{jkl}\bar{u}_{k,l}(\mathbf{x},p) - h_{jk}\bar{\psi}_{,k}(\mathbf{x},p) - \alpha_{jk}\bar{\mu}_{,k}(\mathbf{x},p)\right]n_j.$$

The local integral equation corresponding to the third governing equation (3) has the form

$$\int_{L_s+\Gamma_{sa}} \bar{S}(\mathbf{x},p)d\Gamma = -\int_{\Gamma_{sb}} \bar{\bar{S}}(\mathbf{x},p)d\Gamma, \tag{19}$$

where magnetic flux is given by

$$\bar{S}(\mathbf{x},p)=\bar{B}_j(\mathbf{x},p)n_j(\mathbf{x})=\left[d_{jkl}\bar{u}_{k,l}(\mathbf{x},p)-\alpha_{kj}\psi_{,k}(\mathbf{x},p)-\gamma_{jk}\mu_{,k}(\mathbf{x},p)\right]n_j.$$

In the MLPG method the test and the trial functions are not necessarily from the same functional spaces. For internal nodes, the test function is chosen as a unit step function with its support on the local subdomain. The trial functions, on the other hand, are chosen to be the MLS approximations by using a number of nodes spreading over the domain of influence. According to the MLS [Belytschko et al., (1996)] method, the approximation of the displacement can be given as

$$\mathbf{u}^h(\mathbf{x})=\sum_{i=1}^{m}p_i(\mathbf{x})a_i(\mathbf{x})=\mathbf{p}^T(\mathbf{x})\mathbf{a}(\mathbf{x}),$$

where $\mathbf{p}^T(\mathbf{x})=\{p_1(\mathbf{x}),p_2(\mathbf{x}),\ldots,p_m(\mathbf{x})\}$ is a vector of complete basis functions of order $m$and $\mathbf{a}(\mathbf{x})=\{a_1(\mathbf{x}),a_2(\mathbf{x}),\ldots,a_m(\mathbf{x})\}$ is a vector of unknown parameters that depend on $\mathbf{x}$. For example, in 2-D problems

$$\mathbf{p}^T(\mathbf{x})=\{1,\,x_1,\,x_3\}\qquad\text{for } m=3$$

and

$$\mathbf{p}^T(\mathbf{x})=\left\{1,\,x_1,\,x_3,\,x_1^2,\,x_1x_3,\,x_3^2\right\}\qquad\text{for } m=6$$

are linear and quadratic basis functions, respectively. The basis functions are not required to be polynomials. It is convenient to introduce $r^{-1/2}$ singularity for secondary fields at the crack tip vicinity for modelling of fracture problems [Fleming et al., (1997)]. Then, the basis functions can be considered in the following form

$$\mathbf{p}^T(\mathbf{x})=\left\{1,\,x_1,\,x_3,\,\sqrt{r}\cos\left(\frac{\theta}{2}\right),\,\sqrt{r}\sin\left(\frac{\theta}{2}\right),\,\sqrt{r}\sin\left(\frac{\theta}{2}\right)\sin\theta,\right.$$
$$\left.\sqrt{r}\cos\left(\frac{\theta}{2}\right)\sin\theta\right\}\text{ for } m=7$$

where r and θ are polar coordinates with the crack tip as the origin.

The approximated functions for the Laplace transforms of the mechanical displacements, the electric and magnetic potentials can be written as [Atluri, (2004)]

$$\bar{\mathbf{u}}^h(\mathbf{x},p)=\mathbf{\Phi}^T(\mathbf{x})\cdot\hat{\mathbf{u}}=\sum_{a=1}^{n}\phi^a(\mathbf{x})\hat{\mathbf{u}}^a(p),$$

$$\bar{\psi}^h(\mathbf{x},p)=\sum_{a=1}^{n}\phi^a(\mathbf{x})\hat{\psi}^a(p),$$

$$\bar{\mu}^h(\mathbf{x},p)=\sum_{a=1}^{n}\phi^a(\mathbf{x})\hat{\mu}^a(p), \tag{20}$$

where the nodal values $\hat{\mathbf{u}}^a(p)=(\hat{u}_1^a(p),\hat{u}_3^a(p))^T$, $\hat{\psi}^a(p)$ and $\hat{\mu}^a(p)$ are fictitious parameters for the Laplace transforms of the displacements, the electric and magnetic potentials, respectively, and $\phi^a(\mathbf{x})$ is the shape function associated with the node a. The number of nodes n used for the approximation is determined by the weight function $w^a(\mathbf{x})$. A 4^{th} order spline-type weight function is applied in the present work

$$w^a(\mathbf{x})=\begin{cases}1-6\left(\frac{d^a}{r^a}\right)^2+8\left(\frac{d^a}{r^a}\right)^3-3\left(\frac{d^a}{r^a}\right)^4, & 0\le d^a\le r^a\\ 0, & d^a\ge r^a\end{cases}, \tag{21}$$

where $d^a=\|\mathbf{x}-\mathbf{x}^a\|$ and r^a is the size of the support domain. It is seen that the C^1-continuity is ensured over the entire domain, and therefore the continuity conditions of the tractions, the electric charge and the magnetic flux are satisfied.

The Laplace transform of traction vectors $\bar{t}_i(\mathbf{x},p)$ at a boundary point $\mathbf{x}\in\partial\Omega_s$ are approximated in terms of the same nodal values $\hat{\mathbf{u}}^a(p)$ as

$$\bar{\mathbf{t}}^h(\mathbf{x},p)=\mathbf{N}(\mathbf{x})\mathbf{C}(\mathbf{x})\sum_{a=1}^{n}\mathbf{B}^a(\mathbf{x})\hat{\mathbf{u}}^a(p)+\mathbf{N}(\mathbf{x})\mathbf{L}(\mathbf{x})\sum_{a=1}^{n}\mathbf{P}^a(\mathbf{x})\hat{\psi}^a(p)+\mathbf{N}(\mathbf{x})\mathbf{K}(\mathbf{x})\sum_{a=1}^{n}\mathbf{P}^a(\mathbf{x})\hat{\mu}^a(p), \tag{22}$$

where the matrices $\mathbf{C}(\mathbf{x})$, $\mathbf{L}(\mathbf{x})$ and $\mathbf{K}(\mathbf{x})$ are defined in eq. (10), the matrix **N(x)** is related to the normal vector **n(x)** on $\partial\Omega_s$ by

$$\mathbf{N}(\mathbf{x})=\begin{bmatrix}n_1 & 0 & n_3\\ 0 & n_3 & n_1\end{bmatrix}$$

and finally, the matrices $\mathbf{B}^a$ and $\mathbf{P}^a$ are represented by the gradients of the shape functions as

$$\mathbf{B}^a(\mathbf{x})=\begin{bmatrix}\phi^a_{,1} & 0\\ 0 & \phi^a_{,3}\\ \phi^a_{,3} & \phi^a_{,1}\end{bmatrix},\quad \mathbf{P}^a(\mathbf{x})=\begin{bmatrix}\phi^a_{,1}\\ \phi^a_{,3}\end{bmatrix}.$$

Similarly the Laplace-transform of the normal component of the electric displacement vector $\bar{Q}(\mathbf{x},p)$ can be approximated by

$$\bar{Q}^h(\mathbf{x},p)=\mathbf{N}_1(\mathbf{x})\mathbf{G}(\mathbf{x})\sum_{a=1}^{n}\mathbf{B}^a(\mathbf{x})\hat{\mathbf{u}}^a(p)-\mathbf{N}_1(\mathbf{x})\mathbf{H}(\mathbf{x})\sum_{a=1}^{n}\mathbf{P}^a(\mathbf{x})\hat{\psi}^a(p)-\mathbf{N}_1(\mathbf{x})\mathbf{A}(\mathbf{x})\sum_{a=1}^{n}\mathbf{P}^a(\mathbf{x})\hat{\mu}^a(p), \tag{23}$$

where the matrices $\mathbf{G}(\mathbf{x})$, $\mathbf{H}(\mathbf{x})$ and $\mathbf{A}(\mathbf{x})$ are defined in eq. (11) and

$$\mathbf{N}_1(\mathbf{x}) = \begin{bmatrix} n_1 & n_3 \end{bmatrix}.$$

Eventually, the Laplace-transform of the magnetic flux $\bar{S}(\mathbf{x}, p)$ is approximated by

$$\bar{S}^h(\mathbf{x}, p) = \mathbf{N}_1(\mathbf{x})\mathbf{R}(\mathbf{x}) \sum_{a=1}^{n} \mathbf{B}^a(\mathbf{x})\hat{\mathbf{u}}^a(p) - \mathbf{N}_1(\mathbf{x})\mathbf{A}(\mathbf{x}) \sum_{a=1}^{n} \mathbf{P}^a(\mathbf{x})\hat{\psi}^a(p) - \mathbf{N}_1(\mathbf{x})\mathbf{M}(\mathbf{x}) \sum_{a=1}^{n} \mathbf{P}^a(\mathbf{x})\hat{\mu}^a(p), \quad (24)$$

with the matrices $\mathbf{R}(\mathbf{x})$ and $\mathbf{M}(\mathbf{x})$ being defined in eq. (12).

Satisying the essential boundary conditions and making use of the approximation formula (20), one obtains the discretized form of these boundary conditions as

$$\sum_{a=1}^{n} \phi^a(\boldsymbol{\zeta})\hat{\mathbf{u}}^a(p) = \tilde{\bar{\mathbf{u}}}(\boldsymbol{\zeta}, p) \text{ for } \boldsymbol{\zeta} \in \Gamma_u,$$

$$\sum_{a=1}^{n} \phi^a(\boldsymbol{\zeta})\hat{\psi}^a(p) = \tilde{\psi}(\boldsymbol{\zeta}, p) \text{ for } \boldsymbol{\zeta} \in \Gamma_p,$$

$$\sum_{a=1}^{n} \phi^a(\boldsymbol{\zeta})\hat{\mu}^a = \tilde{\mu}(\boldsymbol{\zeta}, p) \text{ for } \boldsymbol{\zeta} \in \Gamma_a. \quad (25)$$

Furthermore, in view of the MLS-approximation (22) - (24) for the unknown quantities in the local boundary-domain integral equations (16), (18) and (19), we obtain their discretized forms as

$$\sum_{a=1}^{n} \left(\int_{L_s+\Gamma_{st}} \mathbf{N}(\mathbf{x})\mathbf{C}(\mathbf{x})\mathbf{B}^a(\mathbf{x})d\Gamma - \mathbf{I}\rho p^2 \int_{\Omega_s} \phi^a(\mathbf{x})d\Omega \right) \hat{\mathbf{u}}^a(p) + \sum_{a=1}^{n} \left(\int_{L_s+\Gamma_{sq}} \mathbf{N}(\mathbf{x})\mathbf{L}(\mathbf{x})\mathbf{P}^a(\mathbf{x})d\Gamma \right) \hat{\boldsymbol{\psi}}^a(p) + \sum_{a=1}^{n} \left(\int_{L_s+\Gamma_{sb}} \mathbf{N}(\mathbf{x})\mathbf{K}(\mathbf{x})\mathbf{P}^a(\mathbf{x})d\Gamma \right) \hat{\boldsymbol{\mu}}^a(p) = -\int_{\Gamma_{st}} \tilde{\bar{\mathbf{t}}}(\mathbf{x}, p)d\Gamma - \int_{\Omega_s} \bar{\mathbf{F}}(\mathbf{x}, p)d\Omega, \quad (26)$$

$$\sum_{a=1}^{n}\left(\int\limits_{L_s+\Gamma_{sp}}\mathbf{N}_1(\mathbf{x})\mathbf{G}(\mathbf{x})\mathbf{B}^a(\mathbf{x})d\Gamma\right)\hat{\mathbf{u}}^a(p)-\sum_{a=1}^{n}\left(\int\limits_{L_s+\Gamma_{sp}}\mathbf{N}_1(\mathbf{x})\mathbf{H}(\mathbf{x})\mathbf{P}^a(\mathbf{x})d\Gamma\right)\hat{\boldsymbol{\psi}}^a(p)$$
$$-\sum_{a=1}^{n}\left(\int\limits_{L_s+\Gamma_{sp}}\mathbf{N}_1(\mathbf{x})\mathbf{A}(\mathbf{x})\mathbf{P}^a(\mathbf{x})d\Gamma\right)\hat{\boldsymbol{\mu}}^a(p)=-\int\limits_{\Gamma_{sq}}\tilde{Q}(\mathbf{x},p)d\Gamma, \quad (27)$$

$$\sum_{a=1}^{n}\left(\int\limits_{L_s+\Gamma_{sp}}\mathbf{N}_1(\mathbf{x})\mathbf{R}(\mathbf{x})\mathbf{B}^a(\mathbf{x})d\Gamma\right)\hat{\mathbf{u}}^a(p)-\sum_{a=1}^{n}\left(\int\limits_{L_s+\Gamma_{sp}}\mathbf{N}_1(\mathbf{x})\mathbf{A}(\mathbf{x})\mathbf{P}^a(\mathbf{x})d\Gamma\right)\hat{\boldsymbol{\psi}}^a(p)$$
$$-\sum_{a=1}^{n}\left(\int\limits_{L_s+\Gamma_{sp}}\mathbf{N}_1(\mathbf{x})\mathbf{M}(\mathbf{x})\mathbf{P}^a(\mathbf{x})d\Gamma\right)\hat{\boldsymbol{\mu}}^a(p)=-\int\limits_{\Gamma_{sq}}\tilde{S}(\mathbf{x},p)d\Gamma, \quad (28)$$

which are considered on the sub-domains adjacent to the interior nodes as well as to the boundary nodes on Γ_{st}, Γ_{sq} and Γ_{sb}. In equation (26), $\mathbf{I}$ is a unit matrix defined by

$$\mathbf{I}=\begin{pmatrix}1 & 0\\ 0 & 1\end{pmatrix}.$$

Collecting the discretized local boundary-domain integral equations together with the discretized boundary conditions for the displacements, the electrical and magnetic potentials results in the complete system of linear algebraic equations for computation of the nodal unknowns, namely, the Laplace-transforms of the fictitious parameters $\hat{\mathbf{u}}^a(p)$, $\hat{\psi}^a(p)$ and $\hat{\mu}^a(p)$. The time dependent values of the transformed quantities can be obtained by an inverse Laplace-transform. In the present analysis, the Stehfest's inversion algorithm [Stehfest, (1970)] is used. If $\bar{f}(p)$ is the Laplace-transform of $f(t)$, an approximate value f_a of $f(t)$ for a specific time t is given by

$$f_a(t)=\frac{\ln 2}{t}\sum_{i=1}^{N}v_i\bar{f}\left(\frac{\ln 2}{t}i\right), \quad (29)$$

where

$$v_i=(-1)^{N/2+i}\sum_{k=[(i+1)/2]}^{\min(i,N/2)}\frac{k^{N/2}(2k)!}{(N/2-k)!k!(k-1)!(i-k)!(2k-i)!}. \quad (30)$$

In numerical analyses, we have considered $N = 10$ for double precision arithmetic. It means that for each time t we need to solve N boundary value problems for the

corresponding Laplace-transform parameters $p_i = i\ln 2/t$, with $i = 1,2,\ldots,N$. If M denotes the number of the time instants in which we are interested to know $f(t)$, the number of the Laplace- transform solutions $\bar{f}(p_i)$ is then $M \times N$. It should be noted that the present computational method can be easily reformulated into the real time formulation as it was shown recently for 3-D axisymmetric piezoelectric problems in functionally graded materials [Sladek at al., (2008)].

3 Numerical examples

In this section, numerical results for the bending of a square piezoelectric panel are presented to illustrate the accuracy of the proposed method. The square panel with a size $a \times a = 1mm \times 1mm$ made of a PZT-4 material is subjected to a pure bending moment arising from a linearly varying stress at the right boundary (Fig. 1). The lower boundary of the panel is earthed and vanishing electrical potential is assumed on this side of panel. The other boundaries have prescribed vanishing electrical charge.

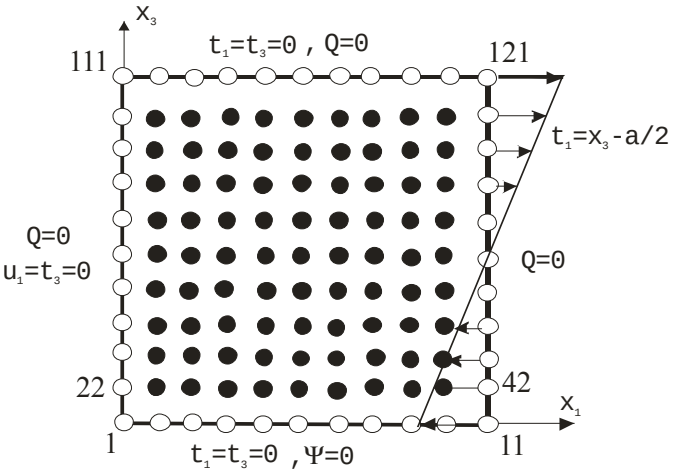

Figure 1: Bending of a square piezoelectric panel

The material coefficients corresponding to PZT-4 material are following

$$c_{11} = 13.9 \cdot 10^{10} Nm^{-2}, \quad c_{13} = 7.43 \cdot 10^{10} Nm^{-2}, \quad c_{33} = 11.3 \cdot 10^{10} Nm^{-2},$$

$$c_{44} = 2.56 \cdot 10^{10} Nm^{-2},$$

$$e_{15} = 13.44 Cm^{-2}, \quad e_{31} = -6.98 Cm^{-2}, \quad e_{33} = 13.84 Cm^{-2},$$

$h_{11} = 6.0 \cdot 10^{-9} C(Vm)^{-1}, \quad h_{33} = 5.47 \cdot 10^{-9} C(Vm)^{-1}.$

The mechanical displacement and the electrical potential fields on the finite square panel are approximated by using 121 (11x11) nodes equidistantly distributed. The local subdomains are considered to be circular with a radius $r_{loc} = 0.08mm$. First, the static boundary conditions are considered. The analytical solution of the problem is given by Parton et al. (1989). Numerical results for the displacement component u_3 and the electric potential along the line $x_3 = a/2$ are presented in Figs. 2 and 3.

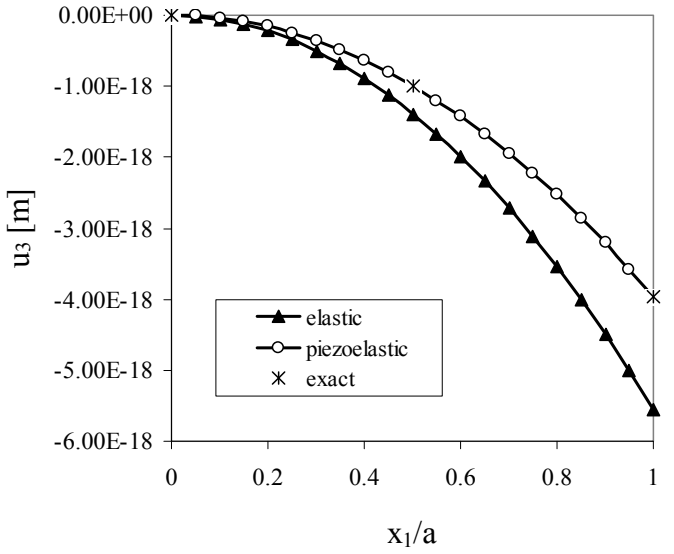

Figure 2: Variation of the mechanical displacement u_3 with normalized coordinate x_1/a

One can observe an excellent agreement of the present results and the exact solution in the whole interval considered. To see the influence of the electrical field on the mechanical displacements the results for a pure elastic panel (without electroelastic interaction$e_{15} = e_{31} = e_{33} = 0$) are given in Fig. 2 too. For the considered boundary conditions, the mechanical displacement component u_3 is reduced in the piezoelectric panel compared to a pure elastic one.

In the next example, we consider the same piezoelectric panel subject to a harmonic load with the angular frequencyω. Both the geometrical and the material parameters are the same as in the previous static case. For the numerical calculations we have used again 441 nodes with a regular distribution. The mass density for

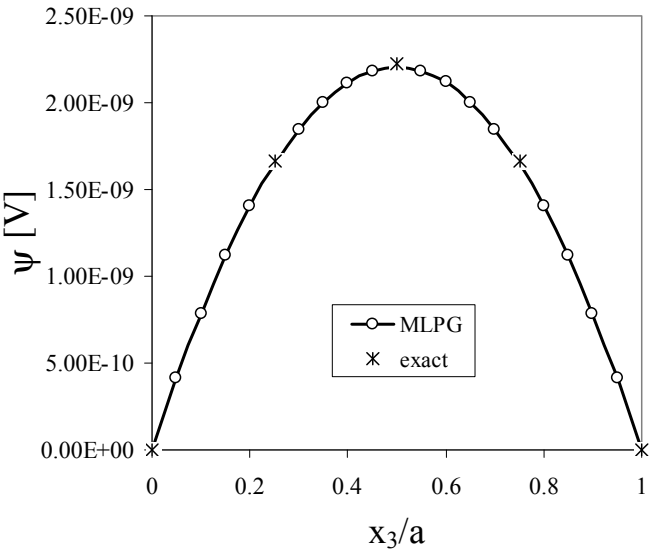

Figure 3: Variation of the electrical potential with normalized coordinate x_3/a

PZT4 piezoelectric material is $\rho = 7500kg/m^3$. Numerical results are compared with those obtained by the FEM-ANSYS computer code. The FEM results have been obtained by using 3600 quadratic eight-noded elements. One can observe quite good agreement of the normalized amplitudes of the beam deflection at the considered angular frequency interval in Fig. 4. The amplitudes are normalized by the static deflection value $u_3^{stat} = 3.96 \cdot 10^{-18}m$. The first eigen-value frequency is $3.8 \cdot 10^6 s^{-1}$.

In the next example the PZT4 actuator is bonded on the upper surface of the steel cantilever beam. The width of the beam and actuators are 40 mm. Other sizes are given in Fig.5. When an external voltage 200V is applied across the thickness of the actuator, the induced strain generates moments that bend the beam.

The variation of the beam deflection with x_1 coordinate is presented in Fig. 6. Quite a good agreement of FEM and MLPG results is observed there. This example is an illustration that the present MLPG method can be successfully applied to problems in piecewise homogeneous structures too.

An edge crack in a finite strip is analyzed in the next example. The sample geometry is given in Fig. 7 with following values: $a = 0.5$, $a/w = 0.4$ and $h/w = 1.2$. Due to the symmetry with respect to x_1 only a half of the specimen is modeled. We have used 930 nodes equidistantly distributed for the MLS approximation of physical fields. On the top of the strip a uniform impact tension σ_0 and electrical

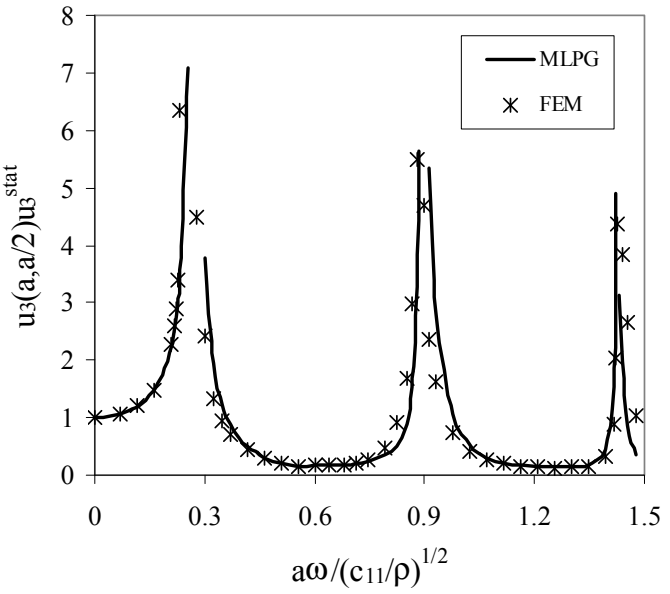

Figure 4: Influence of the angular frequency on the beam deflection

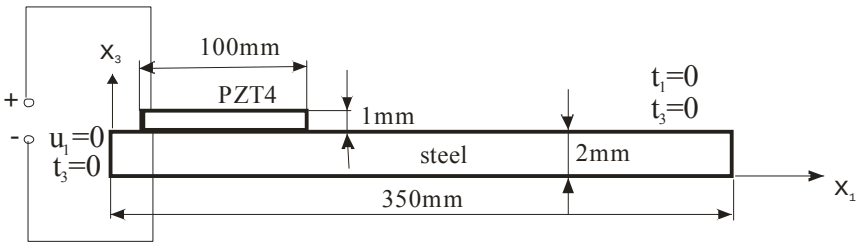

Figure 5: A cantilever beam with piezoelectric actuator

displacement D_0(Heaviside time variation) are applied, respectively. Impermeable electrical boundary conditions on crack surfaces are considered here. Functionally graded material properties in x_1 coordinate are considered. An exponential variation for the elastic, piezoelectric and dielectric tensors is used

$$c_{ijkl}(\mathbf{x}) = c_{ijkl0}\exp(\gamma x_1),$$

$$e_{ijk}(\mathbf{x}) = e_{ijk0}\exp(\gamma x_1)$$

$$h_{ij}(\mathbf{x}) = h_{ij0}\exp(\gamma x_1), \tag{31}$$

where c_{ijkl0}, e_{ijk0} and h_{ij0} correspond to parameters used in the previous example.

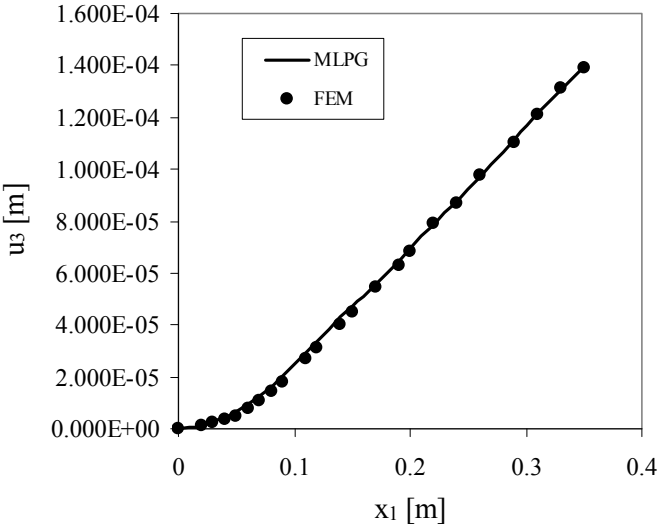

Figure 6: Variation of the beam deflection u_3 with normalized coordinate x_1

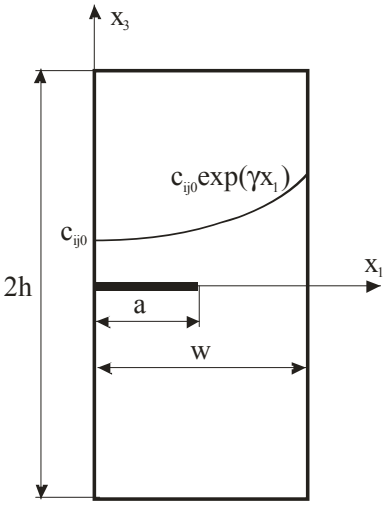

Figure 7: An edge crack in a finite strip with graded material properties in x_1

For cracks in homogeneous and linear piezoelectric and piezomagnetic solids the asymptotic behaviour of the field quantities has been given by Wang and Mai (2003). In the crack tip vicinity, the displacements and potentials show the classical $\sqrt{r}$ asymptotic behaviour. Hence, correspondingly, stresses, the electrical displace-

ment and magnetic induction exhibit $1/\sqrt{r}$behaviour, where r is the radial polar coordinate with origin at the crack tip. Garcia-Sanchez et al. (2007b) extended the approach used in piezoelectricity to magnetoelectroelasticity to obtain asymptotic expression of generalized intensity factors

$$\begin{pmatrix} K_{II} \\ K_I \\ K_E \\ K_M \end{pmatrix} = \sqrt{\frac{\pi}{2r}} \left[Re(\mathbf{B})^{-1} \right] \begin{pmatrix} u_1 \\ u_3 \\ \psi \\ \mu \end{pmatrix} \tag{32}$$

where the matrix $\mathbf{B}$ is determined by the material properties (Garcia-Sanchez et al., 2007b; Garcia-Sanchez and Saez, 2005) and

$$K_I = \lim_{r\to 0} \sqrt{2\pi r}\sigma_{33}(r,0),$$

$$K_{II} = \lim_{r\to 0} \sqrt{2\pi r}\sigma_{13}(r,0),$$

$$K_E = \lim_{r\to 0} \sqrt{2\pi r}D_3(r,0),$$

$$K_M = \lim_{r\to 0} \sqrt{2\pi r}B_3(r,0),$$

are the stress intensity factors (SIF) K_I and K_{II}, K_E is the electrical displacement intensity factor (EDIF), and K_M is the magnetic induction intensity factor (MIIF), respectively.

The influence of the material gradation on the stress intensity factor and electrical displacement intensity factor is analyzed. The temporal variation of the SIF and the EDIF in the cracked strip under a pure mechanical load is presented in Fig. 8 and Fig. 9, respectively. The static stress intensity factor for the considered load and geometry is equal to $K_I^{stat} = 2.642$ Pam$^{1/2}$ and $\Lambda = e_{33}/h_{33}$. Numerical results for a homogeneous strip are compared with FEM ones, and a quite good agreement is observed. For a gradation of mechanical material properties with x_1 coordinate and a uniform mass density, the wave propagation is growing with x_1. Therefore, the peak value of the SIF is reached in a shorter time instant in FGPM strip than in a homogeneous one. The maximum value of the SIF is only slightly reduced for the FGPM cracked strip.

Next, the cracked strip under a pure electrical displacement impact load is analyzed. Since static SIF and EDIF are uncoupled it has to be valid $K_{IV}^{stat} = K_I^{stat}$. The temporal variation of the EDIF is given in Fig. 10. The EDIF is significantly reduced for a cracked FGPM compared to a homogeneous strip. The oscillation of amplitudes for EDIF is again faster in an FGPM strip. Similar phenomena are observed for SIF in Fig. 11

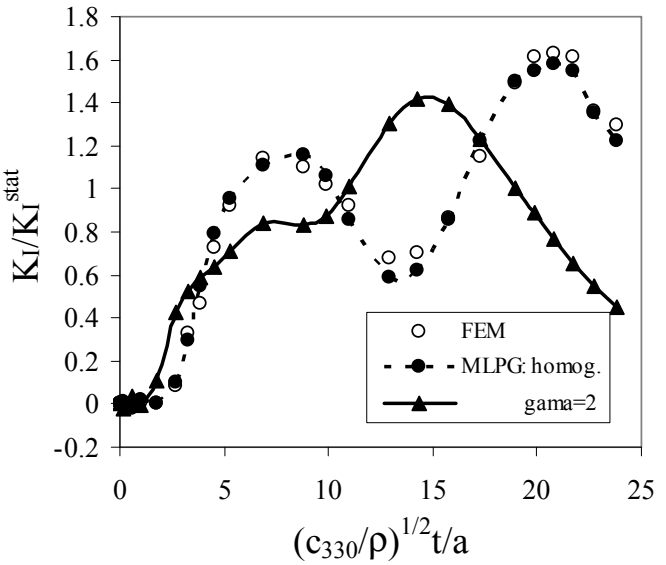

Figure 8: Influence of the material gradation on the stress intensity factor in a cracked strip under a pure mechanical impact load $\sigma_0 H(t-0)$

Next, an edge crack in a finite magneto-electric-elastic strip is analyzed. The geometry of the cracked specimen is the same as in the previous example. We have used again 930 equidistantly distributed nodes for the MLS approximation of the physical fields. On the top of the strip either a uniform tension σ_0, or a uniform magnetic induction B_0 is applied. Firstly, the static loadings are considered. The functionally graded material properties in the x_1-direction are considered. An exponential variation of the elastic, piezoelectric, dielectric, paramagnetic, electromagnetic and magnetic permeability coefficients are assumed as

$$f_{ij}(\mathbf{x}) = f_{ij0}\exp(\gamma_f x_1), \tag{33}$$

where the symbol f_{ij} is commonly used for particular material coefficients with f_{ij0} corresponding to the material coefficients for the $BaTiO_3$ - $CoFe_2O_4$ composite and being given by Li (2000) as

$$c_{11} = 22.6\times 10^{10} Nm^{-2}, \quad c_{13} = 12.4\times 10^{10} Nm^{-2}, \quad c_{33} = 21.6\times 10^{10} Nm^{-2},$$

$$c_{66} = 4.4\times 10^{10} Nm^{-2},$$

$$e_{15} = 5.8 Cm^{-2}, \quad e_{31} = -2.2 Cm^{-2}, \quad e_{33} = 9.3 Cm^{-2},$$

$$h_{11} = 5.64\times 10^{-9} C^2/Nm^2, \quad h_{33} = 6.35\times 10^{-9} C^2/Nm^2,$$

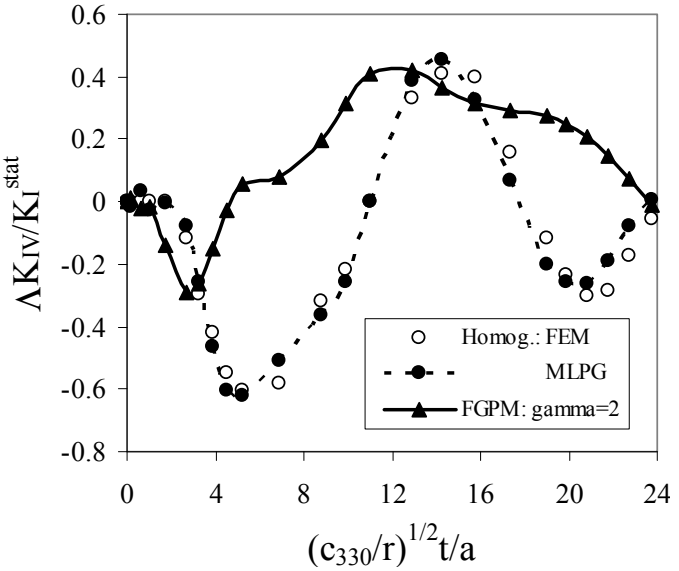

Figure 9: Influence of the material gradation on the EDIF in the cracked strip under a pure mechanical impact load $\sigma_0 H(t-0)$

$d_{15} = 275.0N/Am, \quad d_{21} = 290.2N/Am, \quad d_{22} = 350.0N/Am,$

$\alpha_{11} = 5.367 \times 10^{-12} Ns/VC, \quad \alpha_{33} = 2737.5 \times 10^{-12} Ns/VC,$

$\gamma_{11} = 297.0 \times 10^{-6} Ns^2C^{-2}, \quad \gamma_{33} = 83.5 \times 10^{-6} Ns^2C^{-2}, \quad \rho = 5500kg/m^3$

and the origin $x_1 = 0$ is assumed at the crack tip.

We have considered the same exponential gradient for all coefficients with value $\gamma = 2$ in the numerical calculations. Then, all material parameters at the crack tip are $e^1 = 2.718$ times larger than in the homogeneous material. Then, the crack opening displacement and potentials are significantly reduced in the nonhomogeneous material with gradually increasing material properties in x_1-direction. The normalized stress intensity factors for homogeneous and nonhomogeneous cracked specimen have the following values, $f_I = K_I/\sigma_0\sqrt{\pi a} = 2.105$ and 1.565, respectively. With increasing gradient parameter γ the SIF is decreasing. A similar phenomenon is observed for an edge crack in an elastic FGM strip under a mechanical loading (Dolbow and Gosz, 2002) and for a cracked piezoelectric FGM specimen (Sladek et al., 2007a). For a crack in a homogeneous magneto-electric-elastic solid analyzed in the previous example the SIF, EDIF, magnetic induction intensity factor (MIIF) are uncoupled. However, this conclusion is not valid generally for a continuously nonhomogeneous solid. We have obtained the following normalized

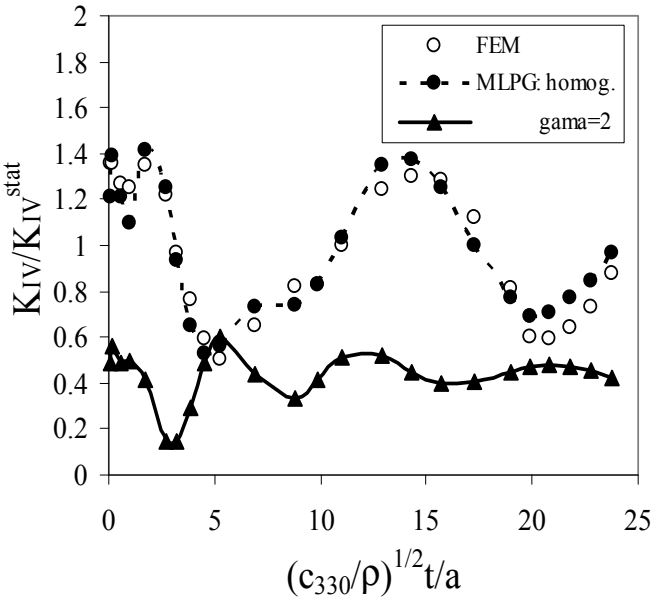

Figure 10: Temporal variation of the EDIF in the cracked strip under a pure electrical displacement impact load $D_0H(t-0)$

quantities: $\Lambda_e K_E/K_I^{stat} = 0.04866$ and $\Lambda_m K_M/K_I^{stat} = 0.00412$. For normalized electrical displacement and magnetic induction intensity factor we have used parameters $\Lambda_e = e_{33}/h_{33}$ and $\Lambda_m = d_{33}/\gamma_{33}$, respectively.

Next, the strip is subjected to an impact mechanical load with Heaviside time variation and the intensity $\sigma_0 = 1$ Pa. The impermeable boundary conditions for the electric displacement and magnetic flux on crack surfaces are considered. The time variation of the normalized stress intensity factor is given in Fig. 12, where $K_I^{stat} = 2.642$ Pam$^{1/2}$. The boundary value problem for a homogeneous material has been analyzed also by the FEM computer code ANSYS. One can observe a quite good agreement of results.

For graded elasticity coefficients along the x_1-coordinate and a uniform mass density, the wave propagation is growing with x_1. Therefore, the peak value of the SIF is reached in a shorter time instant in functionally graded strip than in a homogeneous one. The maximum value of the SIF is only slightly reduced for the FGM cracked strip.

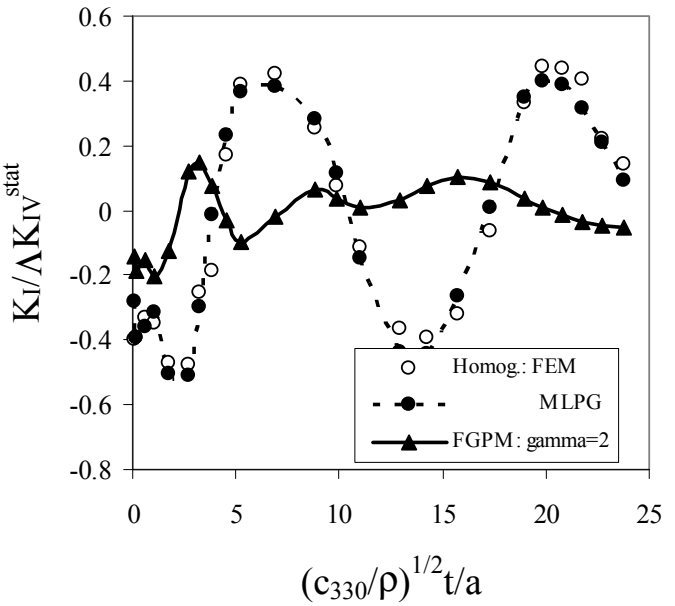

Figure 11: Temporal variation of the SIF in the cracked strip under a pure electrical displacement impact load $D_0H(t-0)$

4 Conclusions

A meshless local Petrov-Galerkin method (MLPG) is presented for modelling of plane piezoelectric and magneto-electric-elastic problems. Both static and impact loads are considered. The Laplace-transform technique is applied to eliminate the time variable in the coupled governing partial differential equations. The analyzed domain is divided into small overlapping circular subdomains. A unit step function is used as the test function in the local weak-form of the governing partial differential equations. The derived local boundary-domain integral equations are non-singular. The moving least-squares (MLS) scheme is adopted for the approximation of the physical field quantities. The proposed method is a truly meshless method, which requires neither domain elements nor background cells in either the interpolation or the integration.

The present method is an alternative numerical tool to many existing computational methods such as the FEM or the BEM. The main advantage of the present method is its simplicity. Compared to the conventional BEM, the present method requires no fundamental solutions and all integrands in the present formulation are regular. Thus, no special numerical techniques are required to evaluate the in-

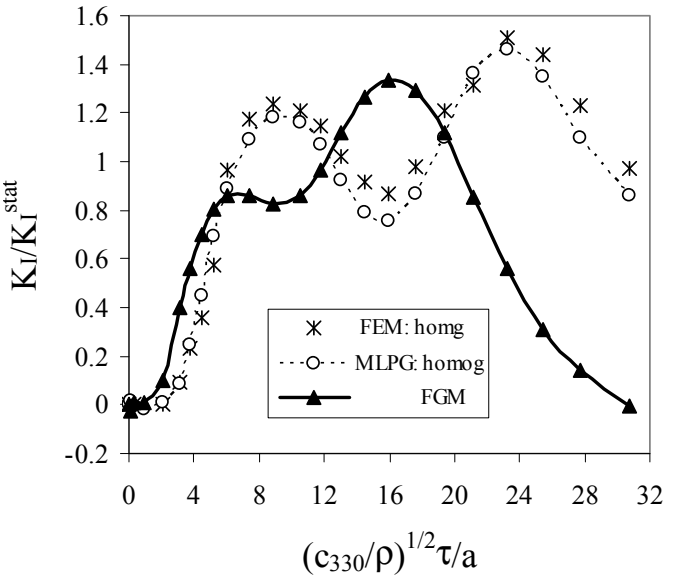

Figure 12: Normalized stress intensity factor for an edge crack in a strip under a pure mechanical load $\sigma_0 H(\tau - 0)$

tegrals. It should be noted here that the fundamental solutions are not available for magneto-electric-elastic solids with continuously varying material properties in general cases. The present formulation also possesses the generality of the FEM. Therefore, the method is promising for numerical analysis of multi-field problems like piezoelectric, electro-magnetic or thermoelastic problems, which cannot be solved efficiently by the conventional BEM.

Acknowledgement: The authors acknowledge the support by the Slovak Science and Technology Assistance Agency registered under number APVV-0427-07, the Slovak Grant Agency VEGA-2/0039/09.

References

Alshits, V.I.; Darinski, A.N.; Lothe, J. (1992): On the existence of surface waves in half-anisotropic elastic media with piezoelectric and piezomagnetic properties. *Wave Motion* 16: 265-283.

Atluri, S.N. (2004): *The Meshless Method, (MLPG) For Domain & BIE Discretizations*, Tech Science Press.

Atluri, S.N.; Sladek, J.; Sladek, V.; Zhu, T. (2000): The local boundary integral

equation (LBIE) and its meshless implementation for linear elasticity. *Comput. Mech*., 25: 180-198.

Atluri, S.N.; Han, Z.D.; Shen, S. (2003): Meshless local Petrov-Galerkin (MLPG) approaches for solving the weakly-singular traction & displacement boundary integral equations. *CMES: Computer Modeling in Engineering & Sciences*, 4: 507-516.

Avellaneda, M.; Harshe, G. (1994): Magnetoelectric effect in piezoelectric/magnetostrictive multilayer (2-2) composites, *Journal of Intelligent Material Systems and Structures* 5: 501-513.

Batra, R.C.; Liang, X.Q. (1997): The vibration of a rectangular laminated elastic plate with embedded piezoelectric sensors and actuators. *Computers and Structures*, 63: 213-216.

Beom, H.G.; Atluri, S.N (1996)., "Near-Tip Fields & Intensity Factors for Interfacial Cracks in Dissimilar Anisotropic Piezoelectric Media," *Int. Journal of Fracture*, 75: 163-183,

Beom H.G.; Atluri S.N. (2002): Conducting cracks in dissimilar piezoelectric media *International Journal of Fracture*, 118 (4): 285-301

Beom H.G.; Atluri S.N. (2003): Effect of electric fields on fracture behavior of ferroelectric ceramics, *Journal of Mechanics and Physics of Solids*, 51 (6): 1107-1125

Belytschko, T.; Krogauz, Y.; Organ, D.; Fleming, M.; Krysl, P. (1996): Meshless methods; an overview and recent developments. *Comp. Meth. Appl. Mech. Engn*., 139: 3-47.

Berlingcourt, D.A.; Curran, D.R.; Jaffe, H. (1964): Piezoelectric and piezomagnetic materials and their function in transducers, *Physical Acoustics* 1: 169-270.

Chen, T.; Lin, F.Z. (1995): Boundary integral formulations for three-dimensional anisotropic piezoelectric solids. *Computational Mechanics*, 15: 485-496.

Chung, M.Y.; Ting, T.C.T. (1995): The Green function for a piezoelectric piezomagnetic anisotropic elastic medium with an elliptic hole or rigid inclusion. *Philos. Mag. Lett.* 72: 405-410.

Ding, H.; Liang, J. (1999): The fundamental solutions for transversaly isotropic piezoelectricity and boundary element method. *Computers & Structures*, 71: 447-455.

Dolbow, J.E.; Gosz, M. (2002): On computation of mixed-mode stress intensity factors in functionally graded materials. *Int. J. Solids Structures* 39: 7065-7078.

Enderlein, M.; Ricoeur, A.; Kuna, M. (2005): Finite element techniques for dynamic crack analysis in piezoelectrics. *International Journal of Fracture*, 134:

191-208.

Eringen, C.E.; Maugin M.A. (1990): Electrodynamics of Continua. Springer-Verlag, Berlin.

Feng, W.J.; Su, R.K.L. (2006): Dynamic internal crack problem of a functionally graded magneto-electro-elastic strip. Int. J. Solids Structures 43: 5196-5216.

Fleming, M.; Chu, Y.A.; Moran, B.; Belytschko, T. (1997): Enriched element-free Galerkin methods for crack tip fields. *International Journal for Numerical Methods in Engineering* 40: 1483-1504.

Gao, C.F., Kessler, H., Balke, H. (2003): Crack problems in magnetoelectroelastic solids. Part I: exact solution of a crack. *International Journal of Engineering Science* 41: 969-981.

Garcia-Sanchez, F.; Saez, A.; Dominguez, J. (2005): Anisotropic and piezoelectric materials fracture analysis by BEM. *Computers & Structures*, 83: 804-820.

Garcia-Sanchez, F.; Zhang, Ch.; Sladek, J.; Sladek, V. (2007a): 2-D transient dynamic crack analysis in piezoelectric solids by BEM. *Computational Materials Science*, 39: 179-186.

Garcia-Sanchez, F.; Rojas-Diaz, R.; Saez, A.; Zhang, Ch. (2007b): Fracture of magnetoelectroelastic composite materials using boundary element method (BEM). *Theoretical and Applied Fracture Mechanics* 47: 192-204.

Gaudenzi, P.; Bathe, K.J. (1995): An iterative finite element procedure for the analysis of piezoelectric continua. Journal of Intelligent Material Systems and Structures, 6: 266-273.

Govorukha, V.; Kamlah, M. (2004): Asymptotic fields in the finite element analysis of electrically permeable interfacial cracks in piezoelectric bimaterials. *Archives Applied Mechanics*, 74: 92-101.

Gruebner, O.; Kamlah, M.; Munz, D. (2003): Finite element analysis of cracks in piezoelectric materials taking into account the permittivity of the crack medium. *Eng. Fracture Mechahanics*, 70: 1399-1413.

Gross, D.; Rangelov, T.; Dineva, P. (2005): 2D wave scattering by a crack in a piezoelectric plane using traction BIEM. *SID: Structural Integrity & Durabil*ity, 1: 35-47.

Ha, S.K.; Keilers, C.; Chang, F.K. (1992): Finite element analysis of composite structures containing distributed piezoceramic sensors and actuators. *AIAA Journal*, 30: 772-780.

Han, F.; Pan, E.; Roy, A.K.; Yue, Z.Q. (2006): Responses of piezoelectric, transversally isotropic, functionally graded and multilayered half spaces to uniform circular surface loading. *CMES: Computer Modeling in Engineering & Sciences*,

14: 15-30.

Hu, K.Q.; Li, G.Q.; Zhong, Z. (2006) Fracture of a rectangular piezoelectromagnetic body. *Mech. Res. Comm.* 33: 482-492.

Kuna, M. (2006): Finite element analyses of cracks in piezoelectric structures – a survey. *Archives of Applied Mechanics*, 76: 725-745.

Landau, L.D.; Lifshitz, E.M. (1984): In: Lifshitz, E.M., Pitaevskii, L.P. (Eds.) *Electrodynamics of Continuous Media* (second edition), Pergamon Press, New York.

Lee, J.S. (1995): Boundary element method for electroelastic interaction in piezoceramics. *Engineering Analysis with Boundary Elements*, 15: 321-328.

Li, J.Y. (2000): Magnetoelectroelastic multi-inclusion and inhomogeneity problems and their applications in composite materials. *International Journal of Engineering Science* 38: 1993-2011.

Liew, K.M.; Lim, H.K.; Tan, M.J.; He, X.Q. (2002): Analysis of laminated composite beams and plates with piezoelectric patches using the element-free Galerkin method. *Computational Mechanics*, 29: 486-497.

Liu, J.X.; Liu, X.L.; Zhao, Y.B. (2001): Green's functions for anisotropic magnetoelectro-elastic solids with an elliptical cavity or a crack. *International Journal of Engineering Sciences* 39: 1405-1418.

Liu, G.R.; Dai, K.Y.; Lim, K.M.; Gu, Y.T. (2002): A point interpolation mesh free method for static and frequency analysis of two-dimensional piezoelectric structures. *Computational Mechanics,* 29: 510-519.

Nan, C.W. (1994): Magnetoelectric effect in composites of piezoelectric and piezomagnetic phases. *Phys. Rev. B*, 50: 6082-6088.

Ohs, R.R.; Aluru, N.R. (2001): Meshless analysis of piezoelectric devices. *Computational Mechanics*, 2**7**: 23-36.

Pan, E. (1999): A BEM analysis of fracture mechanics in 2D anisotropic piezoelectric solids. *Engineering Analysis with Boundary Elements* **23**, 67-76.

Pan, E. (2001) Exact solution for simply supported and multilayered magneto-electro-elastic plates. *ASME J. Applied Mechanics* 68: 608-618.

Parton, V.Z.; Kudryavtsev, B.A. (1988): *Electromagnetoelasticity, Piezoelectrics and Electrically Conductive Solids*. Gordon and Breach Science Publishers, New York.

Parton, V.Z.; Kudryavtsev, B.A.; Senik, N.A. (1989): Electroelasticity. *Applied Mechanics: Soviet Review*, 2: 1-58.

Saez, A.; Garcia-Sanchez, F.; Dominguez, J. (2006): Hypersingular BEM for dynamic fracture in 2-D piezoelectric solids. *Computer Methods in Applied Me-*

chanics and Engineering, 196, pp. 235-246.

Sellountos, E.J.; Polyzos, D. (2003): A MLPG (LBIE) method for solving frequency domain elastic problems. *CMES: Computer Modeling in Engineering & Sciences*, 4: 619-636.

Sellountos, E.J.; Vavourakis, V.; Polyzos, D. (2005): A new singular/hypersingular MLPG (LBIE) method for 2D elastostatics. *CMES: Computer Modeling in Engineering & Sciences*, 7: 35-48.

Sheng, N.; Sze, K.Y. (2006): Multi-region Trefftz boundary element method for fracture analysis in plane piezoelectricity. *Computational Mechanics*, 37: 381-393.

Sladek, J.; Sladek, V.; Atluri, S.N. (2000): Local boundary integral equation (LBIE) method for solving problems of elasticity with nonhomogeneous material properties. *Computational Mechanics*, 24: 456-462.

Sladek, J.; Sladek, V.; Atluri, S.N. (2001): A pure contour formulation for meshless local boundary integral equation method in thermoelasticity, *CMES: Computer Modeling in Engn. & Sciences*, 2: 423-434.

Sladek, J.; Sladek, V.; Van Keer, R. (2003a): Meshless local boundary integral equation method for 2D elastodynamic problems. *Int. J. Num. Meth. Engn.*, 57: 235-249

Sladek, J.; Sladek, V.; Zhang, Ch. (2003b): Application of meshless local Petrov-Galerkin (MLPG) method to elastodynamic problems in continuously nonhomogeneous solids. *CMES: Computer Modeling in Engineering & Sciences*, 4: 637-648.

Sladek, J.; Sladek, V.; Atluri, S.N. (2004): Meshless local Petrov-Galerkin method in anisotropic elasticity. *CMES: Computer Modeling in Engineering & Sciences*, 6: 477-489.

Sladek, J.; Sladek, V.; Wen, P.H.; Aliabadi, M.H. (2006a): Meshless Local Petrov-Galerkin (MLPG) Method for shear deformable shells analysis, *CMES: Computer Modeling in Engineering & Sciences,* 13: 103-118.

Sladek, J.; Sladek, V.; Zhang, Ch.; Garcia-Sanchez, F.; Wunsche, M. (2006b): Meshless local Petrov-Galerkin method for plane piezoelectricity. *CMC: Computers, Materials & Continua*, 4: 109-118.

Sladek, J.; Sladek, V.; Zhang, Ch.; Solek, P.; Starek, L. (2007a): Fracture analyses in continuously nonhomogeneous piezoelectric solids by the MLPG. *CMES: Computer Modeling in Engineering & Sciences,* 19: 247-262 .

Sladek, J.; Sladek, V.; Zhang, Ch.; Solek, P. (2007b): Application of the MLPG to thermo-piezoelectricity. *CMES: Computer Modeling in Engineering & Sciences,* 22: 217-233.

Sladek, J.; Sladek, V.; Solek, P.; Saez, A. (2008): Dynamic 3-D Axisymmet-

ric Problems in Continuously Nonhomogeneous Piezoelectric Solids, *International Journal of Solids and Structures* 45: 4523-4542.

Suresh, S.; Mortensen A. (1998): *Fundamentals of Functionally Graded Materials.* Institute of Materials, London.

Song, Z.F.; Sih, G.C. (2003): Crack initiation behavior in magnetoelectroelastic composite under in-plane deformation. *Theretical Applied Fracture Mechanics* 39: 189-207.

Stehfest, H. (1970): Algorithm 368: numerical inversion of Laplace transform. *Comm. Assoc. Comput. Mach.*, 13: 47-49.

Tian, W.Y.; Gabbert, U. (2005): Macro-crack-micro-crack problem interaction problem in magnetoelectroelastic solids. *Mech. Mater.* 37: 565-592.

Tian, W.Y.; Rajapakse, R.K.N.D. (2005): Fracture analysis of magnetoelectroelastic solids by using path independent integrals. *International Journal of Fracture* 131: 311-335.

Tiersten, H.F. (1969): *Linear Piezoelectric Plate Vibrations*, Plenum Press, New York.

Wang, X.; Shen, Y.P. (2002): The general solution of three-dimensional problems in magnetoelectroelastic media, *International Journal of Engineering Sciences* 40: 1069-1080.

Wang, B.L.; Mai, Y.W. (2003): Crack tip field in piezoelectric/piezomagnetic media. *European Journal of Mechanics A/Solids* 22: 591-602.

Wang, B.L.; Han, J.C.; Mai, Y.W. (2006): Mode III fracture of a magnetoelectroelastic layer: exact solution and discussion of the crack face electromagnetic boundary conditions. *International Journal of Fracture* 139: 27-38.

Wang, B.L.; Mai, Y.W. (2007): Applicability of the crack-face electromagnetic boundary conditions for fracture of magnetoelectroelastic materials. *Int. J. Solids Structures* 44: 387-398.

Zhou, Z.G.; Wang, B.; Sun, Y.G. (2004): Two collinear interface cracks in magneto-electro-elastic composites. *International Journal of Engineering Sciences* 42: 1155-1167.

Zhu, T.; Zhang, J.D.; Atluri, S.N. (1998): A local boundary integral equation (LBIE) method in computational mechanics, and a meshless discretization approaches. *Computational Mechanics* 21: 223-235.

Zhu, X.; Wang, Z.; Meng, A. (1995): A functionally gradient piezoelectric actuator prepared by metallurgical process in PMN-PZ-PT system. *J. Mater. Sci Lett.* 14: 516-518.